Dirac Magnons, Nodal Lines, and Nodal Plane in Elemental Gadolinium

A. Scheie [1,*] Pontus Laurell [2,3,†] P. A. McClarty,[4] G. E. Granroth [1] M. B. Stone [1] R. Moessner,[4] and S. E. Nagler [1,5]

[1]*Neutron Scattering Division, Oak Ridge National Laboratory, Oak Ridge, Tennessee 37831, USA*
[2]*Computational Sciences and Engineering Division, Oak Ridge National Laboratory, Oak Ridge, Tennessee 37831, USA*
[3]*Department of Physics and Astronomy, University of Tennessee, Knoxville, Tennessee 37996, USA*
[4]*Max Planck Institute for the Physics of Complex Systems, Nöthnitzer Str. 38, 01187 Dresden, Germany*
[5]*Quantum Science Center, Oak Ridge National Laboratory, Oak Ridge, Tennessee 37831, USA*

We investigate the magnetic excitations of elemental gadolinium (Gd) using inelastic neutron scattering, showing that Gd is a Dirac magnon material with nodal lines at K and nodal planes at half integer ℓ. We find an anisotropic intensity winding around the K-point Dirac magnon cone, which is interpreted to indicate Berry phase physics. Using linear spin wave theory calculations, we show the nodal lines have nontrivial Berry phases, and topological surface modes. We also discuss the origin of the nodal plane in terms of a screw-axis symmetry, and introduce a topological invariant characterizing its presence and effect on the scattering intensity. Together, these results indicate a highly nontrivial topology, which is generic to hexagonal close packed ferromagnets. We discuss potential implications for other such systems.

Topological materials exhibiting quasiparticles with linear band crossings effectively described by the Dirac equation play an important role at the frontier of condensed matter physics [1,2]. The electronic structure of graphene established it as the prototypical example of a fermionic Dirac material [1,3]. It was subsequently realized that related physics can occur in systems with bosonic quasiparticles including among others phonons [4], photons [5,6], and more recently, magnons [7–12]. The interesting topological features of magnon bands are often associated with band degeneracies that can be understood as a consequence of symmetries describable by spin-space groups [13,14]. Magnon band structures can realize analogs of, e.g., Chern insulators and topological semimetals [10–12] and can host both Dirac [7,8,15] or Weyl magnons [16–20], as well as exhibit extended one-dimensional nodal degeneracies [15,21,22] and triply degenerate points [23]. Consequently, magnetic systems can also exhibit phenomena similar to those found in topological electronic materials, for example, a magnon thermal Hall effect arising from gapped bands with topologically nontrivial Chern numbers [24–29]. In this work we describe a system with a magnon nodal plane degeneracy, thus further extending the fruitful analogy between topological magnets and topological electronic systems [30,31].

Dirac band crossings have been observed in the layered local-moment magnetic systems CrI_3 [32] and $CoTiO_3$ [33,34]. These systems are related to the honeycomb ferromagnet, a simple bipartite lattice that is the prototypical example of a two-dimensional Dirac magnon system. One strong indicator of nontrivial topology is an anisotropic "winding" intensity around the Dirac point, as

seen in $CoTiO_3$ [35,36]. Dirac magnons have also been observed in the three-dimensional antiferromagnet Cu_3TeO_6 [37,38].

In this Letter we use inelastic neutron scattering to measure the magnon spectrum of elemental gadolinium (Gd), showing directly that it is a Dirac material. Gd is a highly isotropic ferromagnet with the hexagonal close packed (hcp) structure that forms a simple three-dimensional bipartite lattice. We demonstrate experimentally that the magnon bands in Gd (i) exhibit Dirac nodal lines with a clear anisotropic winding intensity and nontrivial Berry phase, and (ii) interestingly also show a nodal plane. We discuss the protection of the nodal plane by a combination of a screw-axis symmetry and effective time reversal symmetry, and introduce a $\mathbb{Z}_2$ topological invariant to characterize it. Our results suggest that the entire class of rare earth hcp ferromagnets is a simple model system for topological magnetism.

The Gd hcp structure and its reciprocal lattice are illustrated in Fig. 1. Gd orders ferromagnetically at $T_c = 293$ K [39–41]. Although Gd is metallic, the first three valence electrons are completely itinerant and the rest are localized, leaving an effective Gd^{3+} at each site [42]. In the half-filled f shell, the orbital angular momentum is effectively quenched leaving $S = 7/2$ magnetism [43] with near-perfect isotropy and spin-orbit coupling that vanishes to first order. (Small anisotropies do exist in Gd [44] which influence the direction of the ordered moment [40], but these are of the order 30 μeV [45]—so small that they have never been measured with neutrons.) This makes Gd an ideal material for studying Heisenberg exchange on a hexagonal lattice.
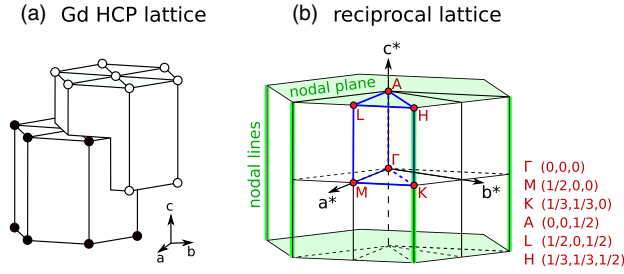
FIG. 1.   (a) hcp crystal structure of Gd. The lattice is bipartite, with interpenetrating layers of *ABAB*-stacked triangular lattices. (b) First Brillouin zone of Gd. The dark blue lines delineate the asymmetric unit in reciprocal space, the red dots show the high symmetry points (notated on the right), and the green regions indicate nodal lines at $h = k = 1/3$ and nodal planes at $\ell = \pm 1/2$.

The Gd spin wave spectrum was first measured by Koehler *et al.* in 1970 [46]; but only along the $(hh0)$, $(h\bar{h}0)$, $(h00)$, and (00ℓ) directions. These data show a linear magnon band crossing at $K = (1/3, 1/3, 0)$, indicating a Dirac node and suggesting the possibility of nontrivial topology. The temperature dependence of the Gd magnons was measured in the 1980s [47,48], but only along the same symmetry directions as Ref. [46]. Here we have used SEQUOIA, a modern time-of-flight spectrometer [49,50] at the SNS [51], to measure the Gd inelastic neutron spectrum over the entire Brillouin zone volume. The sample was a 12 g isotopically enriched ^{160}Gd single crystal (in fact, the same 99.99% enriched crystal as was used in Ref. [46]; naturally occurring Gd is highly neutron absorbing) aligned with the $hh\ell$ plane horizontal. Measurements were carried out at 5 K with incident energies $E_i = 50$ and 100 meV. Data were processed with *Mantid* software [52]; see the Supplemental Material [53] and Ref. [54] for further details. The resulting full dataset allows one to directly see topological features in the spectrum. The data were thoroughly analyzed to determine an accurate spin exchange Hamiltonian: this is discussed in detail in a separate paper [54] focusing on the Gd magnetic interactions. Here we focus on the topological properties of the Gd magnon bands.

Data along high-symmetry directions are shown in Fig. 2 alongside the linear spin wave theory (LSWT) fit. As this comparison demonstrates, the refined model closely reproduces the measured spectrum. Because of this agreement and the high spin length ($S = 7/2$), LSWT is expected to provide a good description of Gd.

From a topology perspective, there are two particularly noteworthy features in the Gd scattering: a nodal line degeneracy at $h = k = 1/3$ extending along ℓ, and a nodal plane degeneracy at $\ell = 1/2$. We will discuss each in turn.

The first feature in the data is a linear band crossing at K, shown in Fig. 2. As shown in Fig. 3, it extends along ℓ, making it a nodal line. This band crossing shows an anisotropic intensity pattern [Figs. 2(e)–2(h)], where the
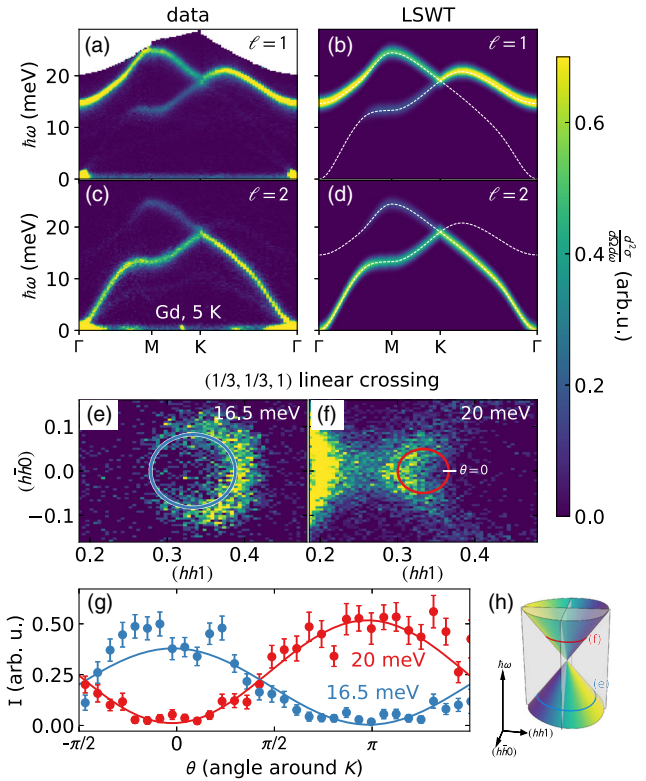

FIG. 2.   Measured and fitted spin wave spectra of Gd. Panels (a) and (c) show the measured Gd spectra along high-symmetry directions. Panels (b) and (d) show spin wave theory calculated spectra using the best fit Hamiltonian [54]. The top row shows the scattering at $\ell = 1$, the second row at $\ell = 2$. Note the linear band crossing at K. Panels (e) and (f) show constant energy slices above and below the band crossing, showing "intensity arcs." Panel (g) shows the intensity binned around the circles in (e) and (f), fitted to a sin function. (h) The "Dirac node" dispersion surface, with colored circles indicating the slices in panels (e)–(f).

intensity follows sinusoidal modulation winding around the Dirac cone, inverted above and below the crossing point. A similar intensity winding was seen in CoTiO$_3$ [33,34], and is understood to be a signature of the nodal line and nontrivial Berry phase around $(1/3, 1/3, \ell)$ [35,36]. (This is similar to a signature of Berry phase physics in graphene seen using polarization-dependent angle-resolved photoemission spectroscopy [55].) Unlike CoTiO$_3$, the offset angle of the intensity winding is zero to within error bars: no anisotropy or off-diagonal exchange shifts the intensity away from the $(hh0)$ line.

To more firmly establish the topological nature of the nodal line, we turn to linear spin-wave theory [56,57] and a simplified $J_1 - J_2 - J_3$ model that qualitatively captures the main features of the full fitted model, including the band crossings,

$$H = J_1 \sum_{\langle i,j \rangle} \mathbf{S}_i \cdot \mathbf{S}_j + J_2 \sum_{\langle\langle i,j \rangle\rangle} \mathbf{S}_i \cdot \mathbf{S}_j + J_3 \sum_{\langle\langle\langle i,j \rangle\rangle\rangle} \mathbf{S}_i \cdot \mathbf{S}_j, \quad (1)$$

where J_n represents the nth nearest neighbor exchange. $J_n < 0$ indicates ferromagnetic exchange. (For the values of the exchange couplings, see Ref. [54].) J_1 and J_3 couple the two sublattices, whereas J_2 couples only sites within the same sublattice (within ab planes). This model includes three of the four largest magnitude exchange interactions that were determined in the full fit. (Since J_4 has a lower coordination number than $J_{1,2,3}$, it only produces a smaller ℓ-dependent contribution to the energy.) Details of these calculations are shown in the Supplemental Material [53].

The hcp lattice is inversion symmetric, and the spin-wave Hamiltonian has an effective time-reversal symmetry [17,53]. Together, these symmetries guarantee that the Berry curvature vanishes everywhere, and thus hcp Gd does not have non-trivial Chern numbers or Weyl magnons. Nevertheless, the same symmetries protect the magnon nodal lines, which are pinned to Brillouin zone corners by threefold rotation symmetry about $\hat{c}$, C_{3z}. The topology of the magnon nodal lines can be classified in terms of the Berry phase about a closed contour $\mathcal{C}$,

$$\gamma_m[\mathcal{C}] = \oint_{\mathcal{C}} d\mathbf{k} \cdot \mathcal{A}_m(\mathbf{k}), \qquad (2)$$

where $\mathcal{A}_m = i\langle u_m(\mathbf{k})|\nabla_{\mathbf{k}}|u_m(\mathbf{k})\rangle$ is the Berry connection, and $|u_m(\mathbf{k})\rangle \sim [\mp \exp(i\phi_{\mathbf{k}}), 1]^T$ is the mth energy eigenstate of the magnon Hamiltonian. If $\mathcal{C}$ is pierced once by a nodal line, it is trivial if $\gamma_m = 0$ and nontrivial if $\gamma_m = \pi$. Direct evaluation for Eq. (1) for Gd shows $\gamma_m[\mathcal{C}] = \pm\pi$ for contours surrounding the nodal lines at K and K' [53], thus demonstrating their topological nature. It is the nontrivial phase $\phi_{\mathbf{k}}$ of the wave function $|u_m(\mathbf{k})\rangle$ that generates the Berry phase and the anisotropic intensity, which is proportional to $1 \pm \cos(\phi_{\mathbf{k}})$ (plus sign for upper band) and winds about K [53].

A second noteworthy feature is a nodal plane. As shown in Fig. 3, the Dirac cone flattens and then inverts as ℓ increases (plotting between $\ell = 1$ and $\ell = 2$—the cone at $\ell = 0$ is not fully visible due to kinematic constraints of the experiment). In fact, every integer shift in ℓ brings an inversion in the Dirac cone intensity, and every half-integer ℓ gives a degeneracy in the modes at all h and k. This degeneracy, shown in Figs. 3(e) and 3(f) where the Dirac cone is completely flattened, gives rise to a nodal plane. Above and below this nodal plane, there is a discontinuous shift in the Dirac cone intensity. This is caused by the phase $\phi_{\mathbf{k}}$ discontinuously flipping by π upon passing through the nodal plane. As we discuss in detail in the Supplemental Material [53], this nodal plane arises in the hcp ferromagnet from the combination of effective time-reversal and non-symmorphic twofold screw symmetry $\{C_{2z}, (0, 0, 1/2)\}$, connecting the two sublattices. Spin orientation plays no role in the Heisenberg limit. Any magnetic Hamiltonian which maintains these symmetries will also have a symmetry-protected nodal plane.
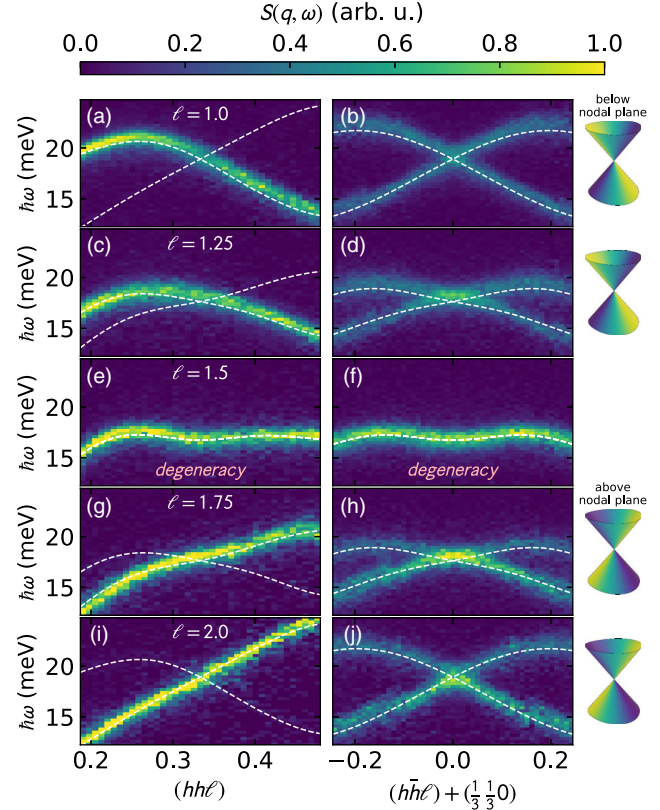

FIG. 3. Evolution of the Dirac cone at $K = ((1/3)(1/3)\ell)$ as a function of ℓ. The white dashed lines are calculations using the fitted LSWT Hamiltonian, while the background color map shows experimental neutron scattering data. The two columns show perpendicular cuts through the K point. As ℓ goes from 1 to 2, the cone flattens and inverts, such that the intensity at $\ell = 1$ is opposite of $\ell = 2$. The two LSWT bands are degenerate at K throughout this evolution, yielding a nodal line. Note the emergence of a nodal plane at $\ell = 1.5$, where the two magnon bands degenerate everywhere in the hk plane. To the right are schematics of the Dirac cone, where intensity inverts after crossing the nodal plane.

We can describe the nodal plane more formally by defining a $\mathbb{Z}_2$ topological invariant, which changes discontinuously across the nodal plane. Such an invariant can either be defined in terms of the Pfaffian of a transformed magnon Hamiltonian [53], or in terms of wave function properties. Here we focus on the latter. We define $\nu_{\mathbf{k}}^m \equiv \mathrm{sgn}\langle u_m(\mathbf{k})|\sigma_1|u_m(\mathbf{k})\rangle$, where σ_1 is the first Pauli spin matrix. If we choose a reference wave vector $\mathbf{k}$ and $\mathbf{k}' \equiv \mathbf{k} + (0, 0, \delta k_z)$ the difference $1/2|\nu_{\mathbf{k}} - \nu_{\mathbf{k}'}|$ counts the number of times the nodal plane is crossed (and thus the number of times the intensity inverts) modulo two.

Although the nodal plane is not expected to produce a topological surface state [31,58], the nodal lines are. To investigate this, we theoretically considered the simplest geometry for surface modes: a slab of a finite number of triangular lattice layers along $\hat{c}$ as shown in Fig. 1. This was done for the full fitted LSWT model (26 neighbor exchange
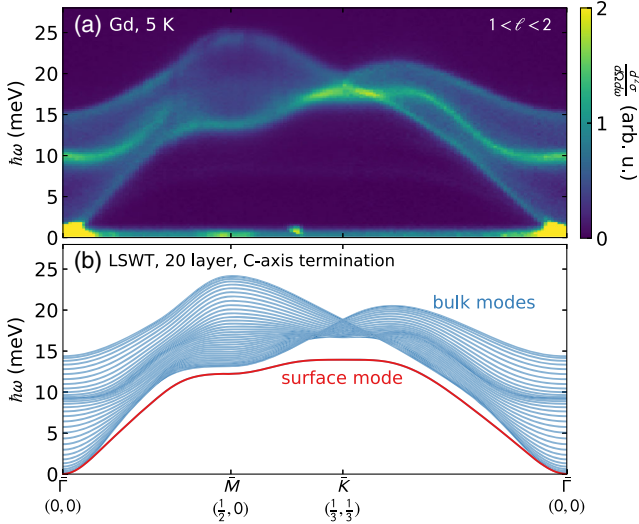
FIG. 4. Surface magnons in Gd. (a) In-plane high-symmetry cuts of 5 K Gd scattering integrated from $\ell = 1$ to $\ell = 2$. (b) Linear spin wave theory calculated modes for a 20-layer Gd slab using the best fit Hamiltonian. Note that, because of the finite extent along $\hat{c}$, ℓ is no longer a good quantum number, and the magnon modes from each layer form a continuum between $\ell = 1$ and $\ell = 2$, such that the magnon modes strongly resemble the integrated data in panel (a). The c-axis termination surface magnon mode, shown in red, lies outside this continuum at lower energies, and is thus distinct from bulk magnons.

terms) using the *SpinW* software [59] by creating a super-cell geometry with and without periodic boundary conditions in the c direction (the c termination was generated by creating a blank space at the top of the physical layers, effectively breaking periodicity). The result is shown in Fig. 4 for 20 Gd unit cells (40 triangular lattice layers). LSWT [Fig. 4(b)] shows the presence of a clear surface mode, emerging from the bulk modes projected into the 2D surface Brillouin zone. Since inelastic neutron scattering is not a surface probe we cannot resolve the same mode in the data, but nevertheless find qualitative agreement with the bulk modes [Fig. 4(a)].

It should be emphasized that neither of these degeneracies —the nodal line at $h = k = 1/3$ and the nodal plane at $\ell = 1/2$—depend sensitively upon the details of the magnetic exchange Hamiltonian. On the hcp lattice, they appear with both the simplest nearest neighbor ferromagnetic exchange interaction, or with any number of further neighbor exchanges—so long as they are all Heisenberg exchanges and the ground state remains ferromagnetic, preserving effective time-reversal symmetry (this was first noted by Brinkman in 1967 [13] and the topological consequences have been explored in Ref. [14]). Thus, although the further neighbor exchange interactions are important for understanding the wiggles in Gd's magnon dispersion, they are not important for understanding the topology.

These experiments and calculations were carried out on Gd, which has near-perfect isotropic Heisenberg exchange.

However, because of the intrinsic connection between symmetry, degeneracy, and topology [13,14,60–62] similar topological features can be expected in more anisotropic ferromagnetic hcp metals such as Tb [63,64], Dy [63,65], and hexagonal Co [66]. (However, for Co one must consider the effects of itinerancy and continuum scattering likely eliminate the observability of Dirac magnons in hcp Co [67–69].) From a topological magnon perspective, it is particularly interesting to consider the addition of inter-actions breaking the symmetries protecting the nodal degeneracies. One choice which can break the effective time-reversal symmetry is the Dzyaloshinskii-Moriya (DM) exchange interaction [70]

$$H = \sum_{ij} \mathbf{D} \cdot (\mathbf{S_i} \times \mathbf{S_j}), \qquad (3)$$

where $\mathbf{D}$ is the DM vector. Like on the honeycomb lattice [12], it is symmetry allowed on the hcp lattice second nearest neighbor bonds.

It is easily shown on the level of LSWT that easy axis or easy plane single-ion anisotropy preserves the extended degeneracies as the effective time reversal symmetry, originating from spin-space symmetries, is preserved, whereas DM exchange with out-of-plane $\mathbf{D}$ vector lifts the K-point and nodal plane degeneracy while leaving a grid of $\ell = 1/2$ nodal lines, giving rise to potential chiral surface magnon modes [54]. However, the true situation is more complicated for anisotropic rare earth hcp ferromagnets such as Tb or Dy. In such cases, the strong spin-orbit coupling may induce other symmetry-allowed off-diagonal exchange, which would in turn affect the surface modes. This means that that inducing chiral surface modes in these materials may prove a challenge. Full characterization of other hcp ferromagnets spin exchange Hamiltonian is necessary to determine the possibility of directional surface modes.

In conclusion, we have shown that the magnetic exci-tation spectrum of elemental gadolinium contains nodal line and nodal plane degeneracies, which are directly visible in the experimental data. The nodal line around K shows anisotropic intensity characteristic of nontrivial topology, and Berry phase calculations confirm this to be so. We also identify a nodal plane in the data, derive the symmetry requirements for such a feature, and propose an invariant describing its topology. These results have impli-cations not just for Gd, but for all hcp ferromagnets, as the topological features are generic to the lattice. Other consequences of the hcp topology may exist—particularly concerning the nodal plane—but these are left for future study.

---

*scheieao@ornl.gov
†laurell@utexas.edu

[1] T. Wehling, A. M. Black-Schaffer, and A. V. Balatsky, Adv. Phys. **63**, 1 (2014).
[2] S. Banerjee, D. S. L. Abergel, H. Ågren, G. Aeppli, and A. V. Balatsky, J. Phys. Condens. Matter **32**, 405603 (2020).
[3] A. H. Castro Neto, F. Guinea, N. M. R. Peres, K. S. Novoselov, and A. K. Geim, Rev. Mod. Phys. **81**, 109 (2009).
[4] F. Li, X. Huang, J. Lu, J. Ma, and Z. Liu, Nat. Phys. **14**, 30 (2018).
[5] A. B. Khanikaev, S. H. Mousavi, W.-K. Tse, M. Kargarian, A. H. MacDonald, and G. Shvets, Nat. Mater. **12**, 233 (2013).
[6] L. Lu, Z. Wang, D. Ye, L. Ran, L. Fu, J. D. Joannopoulos, and M. Soljačić, Science **349**, 622 (2015).
[7] J. Fransson, A. M. Black-Schaffer, and A. V. Balatsky, Phys. Rev. B **94**, 075401 (2016).
[8] S. Owerre, J. Phys. Commun. **1**, 025007 (2017).
[9] S. S. Pershoguba, S. Banerjee, J. C. Lashley, J. Park, H. Ågren, G. Aeppli, and A. V. Balatsky, Phys. Rev. X **8**, 011010 (2018).
[10] M. Malki and G. S. Uhrig, Europhys. Lett. **132**, 20003 (2020).
[11] Z.-X. Li, Y. Cao, and P. Yan, Phys. Rep. **915**, 1 (2021).
[12] P. McClarty, arXiv:2106.01430.
[13] W. Brinkman, J. Appl. Phys. **38**, 939 (1967).
[14] A. Corticelli, R. Moessner, and P. McClarty, arXiv:2103.05656.
[15] K. Li, C. Li, J. Hu, Y. Li, and C. Fang, Phys. Rev. Lett. **119**, 247202 (2017).
[16] F.-Y. Li, Y.-D. Li, Y. B. Kim, L. Balents, Y. Yu, and G. Chen, Nat. Commun. **7**, 12691 (2016).
[17] A. Mook, J. Henk, and I. Mertig, Phys. Rev. Lett. **117**, 157204 (2016).
[18] Y. Su, X. S. Wang, and X. R. Wang, Phys. Rev. B **95**, 224403 (2017).
[19] Y. Su and X. R. Wang, Phys. Rev. B **96**, 104437 (2017).
[20] L.-C. Zhang, Y. A. Onykiienko, P. M. Buhl, Y. V. Tymoshenko, P. Čermák, A. Schneidewind, J. R. Stewart, A. Henschel, M. Schmidt, S. Blügel, D. S. Inosov, and Y. Mokrousov, Phys. Rev. Research **2**, 013063 (2020).
[21] A. Mook, J. Henk, and I. Mertig, Phys. Rev. B **95**, 014418 (2017).
[22] S. Owerre, Sci. Rep. **7**, 6931 (2017).
[23] K. Hwang, N. Trivedi, and M. Randeria, Phys. Rev. Lett. **125**, 047203 (2020).
[24] Y. Onose, T. Ideue, H. Katsura, Y. Shiomi, N. Nagaosa, and Y. Tokura, Science **329**, 297 (2010).
[25] T. Ideue, Y. Onose, H. Katsura, Y. Shiomi, S. Ishiwata, N. Nagaosa, and Y. Tokura, Phys. Rev. B **85**, 134411 (2012).
[26] M. Hirschberger, R. Chisnell, Y. S. Lee, and N. P. Ong, Phys. Rev. Lett. **115**, 106603 (2015).
[27] R. Chisnell, J. S. Helton, D. E. Freedman, D. K. Singh, R. I. Bewley, D. G. Nocera, and Y. S. Lee, Phys. Rev. Lett. **115**, 147201 (2015).
[28] R. Chisnell, J. S. Helton, D. E. Freedman, D. K. Singh, F. Demmel, C. Stock, D. G. Nocera, and Y. S. Lee, Phys. Rev. B **93**, 214403 (2016).
[29] P. Laurell and G. A. Fiete, Phys. Rev. B **98**, 094419 (2018).
[30] Q.-F. Liang, J. Zhou, R. Yu, Z. Wang, and H. Weng, Phys. Rev. B **93**, 085427 (2016).
[31] W. Wu, Y. Liu, S. Li, C. Zhong, Z.-M. Yu, X.-L. Sheng, Y. X. Zhao, and S. A. Yang, Phys. Rev. B **97**, 115125 (2018).
[32] L. Chen, J.-H. Chung, B. Gao, T. Chen, M. B. Stone, A. I. Kolesnikov, Q. Huang, and P. Dai, Phys. Rev. X **8**, 041028 (2018).
[33] B. Yuan, I. Khait, G.-J. Shu, F. C. Chou, M. B. Stone, J. P. Clancy, A. Paramekanti, and Y.-J. Kim, Phys. Rev. X **10**, 011062 (2020).
[34] M. Elliot, P. A. McClarty, D. Prabhakaran, R. D. Johnson, H. C. Walker, P. Manuel, and R. Coldea, Nat. Commun. **12**, 3936 (2021).
[35] P. A. McClarty and J. G. Rau, Phys. Rev. B **100**, 100405(R) (2019).
[36] S. Shivam, R. Coldea, R. Moessner, and P. McClarty, arXiv:1712.08535.
[37] W. Yao, C. Li, L. Wang, S. Xue, Y. Dan, K. Iida, K. Kamazawa, K. Li, C. Fang, and Y. Li, Nat. Phys. **14**, 1011 (2018).
[38] S. Bao, J. Wang, W. Wang, Z. Cai, S. Li, Z. Ma, D. Wang, K. Ran, Z.-Y. Dong, D. L. Abernathy, S.-L. Yu, X. Wan, J.-X. Li, and J. Wen, Nat. Commun. **9**, 2591 (2018).
[39] H. E. Nigh, S. Legvold, and F. H. Spedding, Phys. Rev. **132**, 1092 (1963).
[40] J. W. Cable and E. O. Wollan, Phys. Rev. **165**, 733 (1968).
[41] G. Urbain, P. Weiss, and F. Trombe, Compt. rend. **200**, 2132 (1935).
[42] R. M. Moon, W. C. Koehler, J. W. Cable, and H. R. Child, Phys. Rev. B **5**, 997 (1972).
[43] A. F. Kip, Rev. Mod. Phys. **25**, 229 (1953).

[44] S. Abdelouahed and M. Alouani, Phys. Rev. B **79**, 054406 (2009).

[45] J. J. M. Franse and R. Gersdorf, Phys. Rev. Lett. **45**, 50 (1980).

[46] W. C. Koehler, H. R. Child, R. M. Nicklow, H. G. Smith, R. M. Moon, and J. W. Cable, Phys. Rev. Lett. **24**, 16 (1970).

[47] J. W. Cable, R. M. Nicklow, and N. Wakabayashi, Phys. Rev. B **32**, 1710 (1985).

[48] J. W. Cable and R. M. Nicklow, Phys. Rev. B **39**, 11732 (1989).

[49] G. E. Granroth, A. I. Kolesnikov, T. E. Sherline, J. P. Clancy, K. A. Ross, J. P. C. Ruff, B. D. Gaulin, and S. E. Nagler, J. Phys. Conf. Ser. **251**, 012058 (2010).

[50] G. E. Granroth, D. H. Vandergriff, and S. E. Nagler, Physica (Amsterdam) **385–386B**, 1104 (2006).

[51] T. E. Mason et al., Physica (Amsterdam) **385B–386B**, 955 (2006).

[52] O. Arnold et al., Nucl. Instrum. Methods Phys. Res., Sect. A **764**, 156 (2014).

[53] See Supplemental Material at http://link.aps.org/supplemental/10.1103/PhysRevLett.128.097201 for more details of the experiments and calculations.

[54] A. Scheie, P. Laurell, P. A. McClarty, G. Granroth, M. B. Stone, R. Moessner, and S. E. Nagler, companion paper, Phys. Rev. B **105**, 104402 (2022).

[55] C. Hwang, C.-H. Park, D. A. Siegel, A. V. Fedorov, S. G. Louie, and A. Lanzara, Phys. Rev. B **84**, 125422 (2011).

[56] T. Holstein and H. Primakoff, Phys. Rev. **58**, 1098 (1940).

[57] J. Jensen and A. Mackintosh, *Rare Earth Magnetism, Structures and Excitations* (Clarendon Press, Oxford, UK, 1991).

[58] M. Xiao, L. Ye, C. Qiu, H. He, Z. Liu, and S. Fan, Sci. Adv. **6**, eaav2360 (2020).

[59] S. Toth and B. Lake, J. Phys. Condens. Matter **27**, 166002 (2015).

[60] A. P. Cracknell, J. Phys. C **3**, S175 (1970).

[61] P. Narang, C. A. C. Garcia, and C. Felser, Nat. Mater. **20**, 293 (2021).

[62] H. Watanabe, H. C. Po, and A. Vishwanath, Sci. Adv. **4**, 8685 (2018).

[63] P.-A. Lindgård, Phys. Rev. B **17**, 2348 (1978).

[64] H. B. Møller, J. C. G. Houmann, and A. R. Mackintosh, J. Appl. Phys. **39**, 807 (1968).

[65] R. M. Nicklow, N. Wakabayashi, M. K. Wilkinson, and R. E. Reed, Phys. Rev. Lett. **26**, 140 (1971).

[66] T. Perring, A. Taylor, and G. Squires, Physica (Amsterdam) **213B–214B**, 348 (1995).

[67] S.-H. Do, K. Kaneko, R. Kajimoto, K. Kamazawa, M. B. Stone, S. Itoh, T. Masuda, G. D. Samolyuk, E. Dagotto, W. R. Meier, B. C. Sales, H. Miao, and A. D. Christianson, arXiv:2107.08915.

[68] H. Okumura, K. Sato, and T. Kotani, Phys. Rev. B **100**, 054419 (2019).

[69] T. Skovhus and T. Olsen, Phys. Rev. B **103**, 245110 (2021).

[70] T. Moriya, Phys. Rev. **120**, 91 (1960).

[71] United States Department of Energy, 2014, http://energy.gov/downloads/doe-public-access-plan.